

Received September 13, 2024. Accepted November 29, 2024. Published December 19, 2024.

ISSN: 2448-7775

A simplest Padé Approximant-Based Algorithm for Phasor Estimation of Electrical Signals

MARCO A. PEREZ G.¹, RAMON JIMENEZ BETANCOURT^{1*}, EMILIO BAROCIO², JUAN M. GONZALEZ LOPEZ¹, ANTONIO CONCHA SANCHEZ¹.

¹University of Colima, Colima, Colima, México.

²University of Guadalajara, Guadalajara, Jalisco, México.

*Corresponding Author: rjimenez@uacol.mx

ABSTRACT A simplest Padé approximant-based measurement algorithm is proposed for the phasor estimation of electrical signals. Initially, the samples are transformed to the z-domain, and the Padé approximant is obtained. The Padé representation adopts the structure of a single frequency oscillator, where the amplitude, frequency, and phase are explicitly expressed in terms of the samples. The proposed algorithm is tested and compared with other similar approaches using the IEEE C37.118 standard, demonstrating its competitiveness and compliance with all tests. The algorithm is implemented on an IoT board equipped with voltage and current sensors to estimate phasor characteristics at low voltage levels in electrical networks. A web interface enables real-time visualization of the phasor characteristics, affirming the accuracy of the proposed method. The design of the measurement system and the C-code of the Padé method are fully available in a repository for reproduction by others.

KEYWORDS— Padé approximant; IoT; z-transform; phasor measurement unit, web interface.

I. INTRODUCTION

Currently, various methods have been proposed for estimating the phasor of electrical signals [1-10]. However, the Discrete Fourier Transform (DFT) method remains the most widely used in phasor measurement units (PMUs) due to its low computational complexity, which allows it to be implemented on any hardware. This is why most PMU manufacturers continue to rely on it. A key aspect of the DFT is its frequency resolution, as a considerable number of samples per cycle is necessary for accurate phasor determination.

As electrical networks incorporate renewable energy sources, the complexity of phasor estimation becomes a significant challenge. The electrical signals in these networks exhibit characteristics such as inter-harmonics, intermodulation, and frequency ramps, among others. These complexities pose a challenge to the standard use of DFT in phasor estimation, as high frequency resolution or the implementation of digital filters prior to signal processing is required. This necessity compromises the computing time and increases the latency of the PMU. Consequently, variants like Interpolated DFT (IpDFT) and Enhanced Interpolated DFT (E-IPDFT) have been developed to estimate phasors with fewer samples.

Phasor estimation time continues to be a challenge, necessitating algorithms that are computationally efficient and provide tolerable estimation errors. The number of samples required for accurate estimation is critical. In [1], the different processing stages of the PMU are comprehensively described, with a total latency estimated at up to 800 microseconds.

Therefore, reducing the latency of the estimation algorithm remains an area of active research, prompting the development of new phasor estimation methods.

Among the simplest methods for estimating amplitude and frequency is the one based on the Teager-Kaiser operator, which requires only three samples and a high sampling frequency. However, this method cannot estimate the phase, limiting its application to event detection. The Eigenrealization (ERA) method is another low-complexity approach that determines the phasor with a reduced number of samples (at least eight per cycle) and uses a second-order representation to obtain parameters, as demonstrated in [11]. Additionally, the Matrix Pencil (MP) method has proven to be another efficient technique for phasor estimation, characterized by its reduced complexity and quick parameter determination [12].

The motivation for our paper is to present a low-cost measurement system for PMU purposes. Our algorithm, based on the dynamic concept of phasors, is simple and easy to implement, requires fewer computations compared to DFT, meets all the steady-state and dynamic performance criteria of the IEEE Standard [13], performs satisfactorily during system faults, and exhibits a fast response time during significant disturbances. We have also designed a dedicated web interface to display signal information in real-time. The investigations enabled by the proposed measurement system focus on compliance with IEEE standards, monitoring dynamic power signals that change in amplitude and frequency during PMU testing, and estimating reference values for dynamic power signals.

II. METHODOLOGY

Let a single frequency undamped noisy sinusoid signal of the form:

$$v_k = A(kT)\cos(2k\pi fT + \theta(kT)) + \varphi(k) \quad (1)$$

where v_k is the instantaneous amplitude at the time kT , A is the phasor amplitude, f is the frequency, θ is the phase in rads, and $f_s = 1/T$ the sampling frequency. Consider the following vector of N samples identically time spaced, which are acquired during a cycle of the nominal frequency f_o , i.e., during a period of $T=1/(8f_o)$

$$V = [v_0 \ v_1 \ \dots \ v_{N-1}] \quad (2)$$

The z -transform of the samples gives the $(-N+1)$ -order polynomial:

$$V(z^{-1}) = v_0 + v_1 z^{-1} + v_2 z^{-2} + \dots + v_{N-1} z^{-N+1} \quad (3)$$

Now let consider that this polynomial can be expressed by the $L=1, M=2$ Padé Approximant as [20]:

$$\begin{aligned} V(z^{-1}) &= v_0 + v_1 z^{-1} + v_2 z^{-2} + \dots + v_{N-1} z^{-N+1} \\ &= \frac{p_0 + p_1 z^{-1}}{q_0 + q_1 z^{-1} + q_2 z^{-2}} \end{aligned} \quad (4)$$

where the coefficients $p_0, p_1, q_0, q_1,$ and q_2 are unknown. As can be seen, the above Padé approximation permits representing the signal samples by a two-pole transfer function. To obtain the Padé coefficients, Eq. (4) is alternatively expressed as:

$$\begin{aligned} (v_0 + v_1 z^{-1} + \dots + v_{N-1} z^{-N+1})(q_0 + q_1 z^{-1} + q_2 z^{-2}) \\ = p_0 + p_1 z^{-1} \end{aligned} \quad (5)$$

Making the products in Eq. (5) and grouping the terms of same order in z , the next two linear system of equations are obtained [21]:

$$\begin{bmatrix} v_{N-3} & v_{N-2} & v_{N-1} \\ \vdots & \vdots & \vdots \\ v_1 & v_2 & v_3 \\ v_0 & v_1 & v_2 \end{bmatrix} \begin{bmatrix} q_2 \\ q_1 \\ q_0 \end{bmatrix} = \begin{bmatrix} 0 \\ \vdots \\ 0 \\ 0 \end{bmatrix} \quad (6a)$$

$$\begin{bmatrix} v_0 & v_1 \\ 0 & v_0 \end{bmatrix} \begin{bmatrix} q_1 \\ q_0 \end{bmatrix} = \begin{bmatrix} p_1 \\ p_0 \end{bmatrix} \quad (6b)$$

These two linear systems can be solved in simultaneous form. First, if in the homogenous system in Eq. (6a) is setting $q_0=1$, then q_1 and q_2 are given by solution of Eq. (7):

$$\begin{bmatrix} v_{N-3} & v_{N-2} \\ \vdots & \vdots \\ v_1 & v_2 \\ v_0 & v_1 \end{bmatrix} \begin{bmatrix} q_2 \\ q_1 \end{bmatrix} = - \begin{bmatrix} v_{N-1} \\ \vdots \\ v_3 \\ v_2 \end{bmatrix} \quad (7)$$

Pre-multiplying both sides of Eq. (7) by the transpose of

$$\begin{bmatrix} v_{N-3} & v_{N-2} \\ \vdots & \vdots \\ v_1 & v_2 \\ v_0 & v_1 \end{bmatrix} \text{ yields in}$$

$$\begin{aligned} &\begin{bmatrix} v_{N-3} & \dots & v_1 & v_0 \\ v_{N-2} & \dots & v_2 & v_1 \end{bmatrix} \begin{bmatrix} v_{N-3} & v_{N-2} \\ \vdots & \vdots \\ v_1 & v_2 \\ v_0 & v_1 \end{bmatrix} \begin{bmatrix} q_2 \\ q_1 \end{bmatrix} \\ = &- \begin{bmatrix} v_{N-3} & \dots & v_1 & v_0 \\ v_{N-2} & \dots & v_2 & v_1 \end{bmatrix} \begin{bmatrix} v_{N-1} \\ \vdots \\ v_3 \\ v_2 \end{bmatrix} \end{aligned} \quad (8)$$

Making the products is obtained Eq. (9)

$$\begin{bmatrix} \sum_{k=0}^{N-3} v_k^2 & \sum_{k=0}^{N-3} v_k v_{k+1} \\ \sum_{k=0}^{N-3} v_k v_{k+1} & \sum_{k=1}^{N-2} v_k^2 \end{bmatrix} \begin{bmatrix} q_2 \\ q_1 \end{bmatrix} = - \begin{bmatrix} \sum_{k=0}^{N-3} v_k v_{k+2} \\ \sum_{k=1}^{N-2} v_k v_{k+1} \end{bmatrix} \quad (9)$$

Solution of (9) give the q 's coefficients as:

$$q_2 = \frac{\sum_{k=0}^{N-3} v_k v_{k+1} \sum_{k=1}^{N-2} v_k v_{k+1} - \sum_{k=1}^{N-2} v_k^2 \sum_{k=0}^{N-3} v_k v_{k+2}}{\sum_{k=0}^{N-3} v_k^2 \sum_{k=1}^{N-2} v_k^2 - (\sum_{k=0}^{N-3} v_k v_{k+1})^2} \quad (10a)$$

$$q_1 = \frac{\sum_{k=0}^{N-3} v_k v_{k+2} \sum_{k=0}^{N-3} v_k v_{k+1} - \sum_{k=0}^{N-3} v_k^2 \sum_{k=1}^{N-2} v_k v_{k+1}}{\sum_{k=0}^{N-3} v_k^2 \sum_{k=1}^{N-2} v_k^2 - (\sum_{k=0}^{N-3} v_k v_{k+1})^2} \quad (10b)$$

Then the solution for Eq. (6b) is straightforward and the coefficients p_0 and p_1 becomes:

$$p_0 = v_0 \quad p_1 = v_1 + v_0 q_1 \quad (11)$$

Knowing the coefficients p_0, p_1, q_0, q_1 and q_2 , the Padé representation can be expressed in the pole-residue representation as follows [22]:

$$\begin{aligned} &\frac{p_0 + p_1 z^{-1}}{q_0 + q_1 z^{-1} + q_2 z^{-2}} \\ = &\frac{r_1}{1 - \alpha_1 z^{-1}} + \frac{r_2}{1 - \alpha_2 z^{-1}} \end{aligned} \quad (12)$$

where α_1 and α_2 are the poles, whilst r_1 and r_2 are the residues. These terms are given by:

$$\alpha_{1,2} = \frac{1}{2} \left(-q_1 \pm j \sqrt{4q_2 - q_1^2} \right) \quad (13)$$

$$r_{1,2} = \frac{1}{2} \left(p_0 \pm j \frac{p_0 q_1 - 2p_1}{\sqrt{4q_2 - q_1^2}} \right) \quad (14)$$

Since the proposed model in Eq. (12) represents an oscillator, the parameters of the signal can be obtained from Eqs. (13) and (14) as [14]:

$$\text{Amplitude: } A = 2\|r_1\| \text{ V} \quad (15a)$$

$$\text{Frequency: } f = f_s \frac{4\alpha_1}{2\pi} \text{ Hz} \quad (15b)$$

$$\text{Phase: } \theta = \angle r_1 \text{ rad} \quad (15c)$$

$$\text{Damping: } \sigma = f_s \log_e \|\alpha_1\| \text{ s}^{-1} \quad (15d)$$

Using the parameters, A and θ , we can write the phasor for the proposed model as follows:

$$\mathbf{V} = A\angle\theta = V'_r + jV'_i \quad (16)$$

where X'_r and X'_i represent the real and imaginary part of the phasor, respectively.

A. IDENTIFICATION OF FREQUENCY DEVIATIONS

In the more general condition, the samples do not satisfy the ideal conditions, i.e., noise and harmonic distortion are present, thus under real conditions, the signal frequency is determined by:

$$f = \frac{f_s}{2\pi} \text{atan} \left(\frac{\sqrt{4q_2 - q_1^2}}{q_1} \right) \quad (17)$$

Note that the estimation of the frequency is strongly related with the coefficient q_1 , thus when a significant change of this coefficient occurs a deviation of the nominal frequency appearing. Positive (negative) value of q_1 implies an increase (decrease) in the frequency of the signal.

B. IDENTIFICATION OF AMPLITUDE DEVIATIONS

The amplitude of the phasor is strictly determined by the magnitude of the residues r_1 and r_2 , i.e.

$$A = \sqrt{p_0^2 + \frac{(p_0q_1 - 2p_1)^2}{4q_2 - q_1^2}} \quad (18)$$

Note that denominator $4q_2 - q_1^2$ can be used for identification of sudden variations on the signal amplitude. Decreasing $4q_2 - q_1^2$ indicate that the amplitude A is increasing, and vice versa.

C. IDENTIFICATION OF PHASE DEVIATIONS

According to the definition for the phase give in Eq. (15c), the angle of Eq. (14) becomes:

$$\underline{\theta} = \text{atan} \left(\frac{p_0q_1 - 2p_1}{p_0\sqrt{4q_2 - q_1^2}} \right) \text{ rad} \quad (19)$$

The phase varies continuously with the change of instantaneous frequency and rotates once every four new

samples. The next expression illustrates the relationship between this phase and the instantaneous frequency:

$$\theta = \underline{\theta} - (m - 1) \frac{2\pi(f - f_0)}{f_0}, \quad m = 0, 1, \dots \quad (20)$$

where m refers to the window under analysis, and f_0 is the nominal frequency.

D. IDENTIFICATION OF DAMPING DEVIATIONS

The damping of the signal can be calculated by assuming a decrease in amplitude according to its exponential nature.

$$\sigma = f_s \log_e(q_2) \text{ s}^{-1} \quad (21)$$

Note that it depends only on the coefficient q_2 . This damping becomes zero when $q_2=1$, whilst it is negative when q_2 is in the range $0 < q_2 < 1$, and positive when $q_2 > 1$.

III. SIMULATION RESULTS

This section is devoted to testing the proposed algorithm with synthetic signals that satisfy the features mentioned in the IEEE Std C37.118.1-2011 [13].

I.e., 1. Tolerance to noise; 2. Harmonic distortion; 3. Interharmonic distortion; 4. Decaying harmonic and DC decaying offset; 5. Amplitude step response; 6. Phase step response; 7. Amplitude and phase modulation. 8. Frequency ramp response. Table I summarize the test signals used.

TABLE I. SIGNALS FOR COMPLIANCE THE IEEE STD C37.118.1-2011 [13].

Signal ¹	Parameters
$v(k) = V_p \cos(k\omega T + \theta) + \varphi(kT)$	$\varphi = 30 \text{ dB}$
$v(k) = V_p \cos(k\omega T) + \frac{1}{2400} V_p \cos(5k\omega T) + \frac{1}{40} V_p \cos(9k\omega T) + \frac{1}{600} V_p \cos(15k\omega T)$	Harmonics of 5 th , 9 th , & 15 th (THD=0.514%)
$v(k) = V_p \cos(k\omega T) + \frac{1}{2400} V_p \cos(1.3k\omega T) + \frac{1}{40} V_p \cos(9.7k\omega T) + \frac{1}{600} V_p \cos(15.2k\omega T)$	Interharmonics of 1.3 th , 9.7 th , & 15.2 th (TIHD=0.514%)
$v(k) = V_p \cos(k\omega T) + \frac{1}{600} V_p e^{-0.1t} (1 + \cos(5k\omega T))$	Decaying harmonic of 5 th plus DC decaying offset
$v(k) = (1 + k_x u(kT)) V_p \cos(2k\pi f T)$	$k_x = 0.1$
$v(k) = V_p \cos(k\omega T + k_a u(kT))$	$k_a = \pi/18 \text{ rad}$
$v(k) = V_p (1 + k_x u(kT) \cos(k\omega_m T)) \cos(k_a u(kT) \cos(k\omega_m T - \pi))$	$f_m = 5 \text{ Hz}$, $k_x = k_a = 0.1$
$v(k) = V_p \cos(2kf\pi T + \pi R_f k^2 T^2)$	$R_f = 1 \text{ Hz/s}$

Note: $V_p = 120\sqrt{2} \text{ V}$, $f = 60 \text{ Hz}$, and $\theta = 0^\circ$.

The Total Vector Error (TVE), Frequency Error (FE) and the Rate of Change of Frequency Error (RFE) are three metrics used to determine the validity of the algorithm, and they are given by:

$$\text{TVE}(m) = \sqrt{\frac{(V_r'(m) - V_r(m))^2 + (V_i'(m) - V_i(m))^2}{(V_r(m))^2 + (V_i(m))^2}} \quad (22)$$

$$\text{FE}(m) = |f - f'| \quad (23)$$

$$\text{RFE}(m) = \frac{df}{dt} - \frac{df'}{dt} \quad (24)$$

where $V_r(m)$ and $V_i(m)$ are the real and imaginary part of the true phasor, respectively. $V_r'(m)$ and $V_i'(m)$ are the real and imaginary part of the computed phasor, respectively; moreover, f is the true frequency and f' is the computed frequency.

The Padé method is compared with the approaches MP, ERA, TKO and DFT. It is important to mention that for ERA and DFT methods were employed eight samples, for MP four samples, and TKO three samples. The next results were obtained over 60 cycles of the fundamental frequency (60 Hz) and $f_s = 480$ Hz.

A. RESULTS OF TVE

Fig. 1 displays the TVE results, with the IEEE C37.118 standard limit (in red). The TKO results are excluded as it doesn't calculate phase angle. The proposed method fully

complies with the standard, but harmonics may raise the TVE, indicating the need for pre-filtering. When a phase step is introduced, an overshoot (over 1) occurs before stabilizing. Thus, the Padé method provides accurate magnitude and phase only under low signal distortion.

B. RESULTS OF FE

Fig. 2 illustrates the FE results, demonstrating that the proposed method complies with the IEEE C37.118 standard in most cases. Notable exceptions include scenarios involving the decaying DC offset (Fig. 2e) and amplitude and phase modulation (Fig. 2h), where the algorithm shows some deviations. These deviations are primarily attributed to the lower sampling rate used in the testing conditions, which impacts the algorithm's accuracy when handling rapidly changing signal dynamics.

C. RESULTS OF RFE

Fig. 3 shows the results for RFE error for all the signals. The derivative of the frequency was obtained using the forward numerical derivative with $h = 1/60$. From these results, it can be observed that the Padé method meets the IEEE test in all cases except for the interharmonic distortion (Fig. 3d), decaying DC offset (Fig. 3e) as well as for amplitude and phase modulation (Fig. 3h). These deviations are likely due to the method's sensitivity to rapidly changing signals or transient components, such as interharmonics and decaying DC offsets.

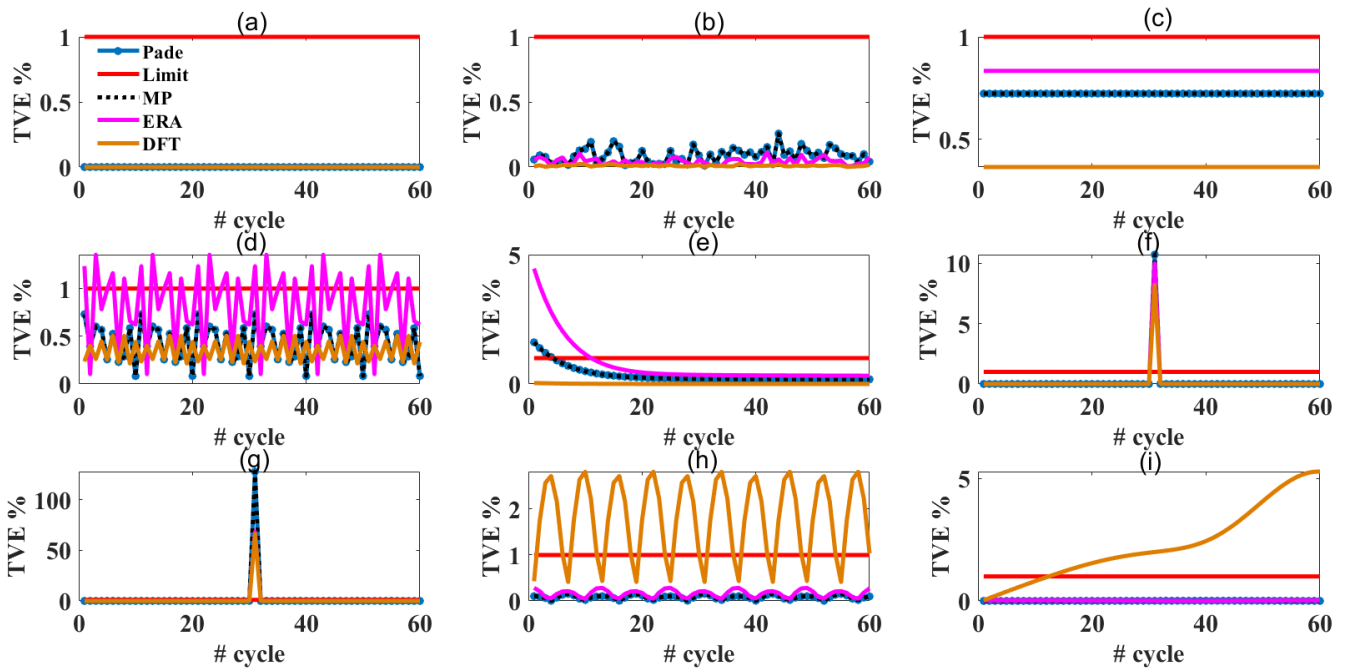


Fig. 1. TVE for the signals under study: (a) Noiseless (b) Tolerance to noise (c) Harmonic distortion (d) Interharmonic distortion (e) Decaying harmonic and DC decaying offset (f) Amplitude step (g) Phase step (h) Amplitude and phase modulation (i) Frequency ramp response.

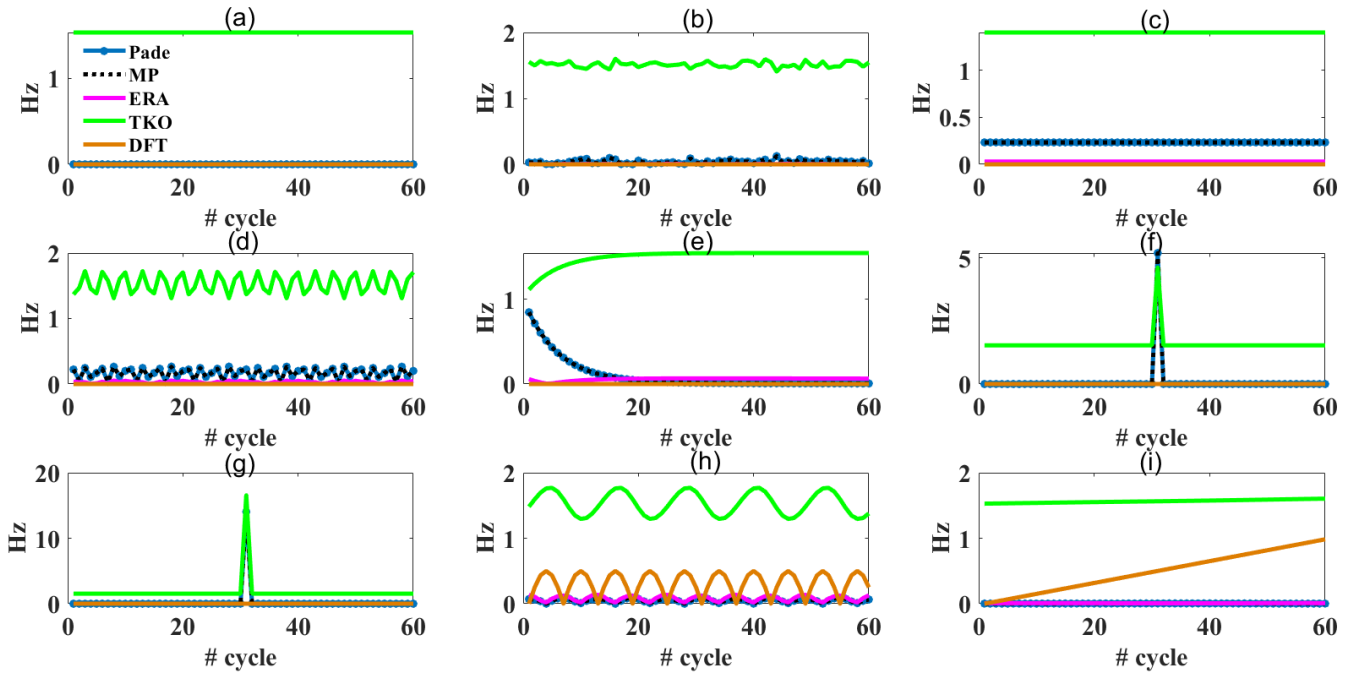


Fig. 2. FE for the signals under study: (a) Noiseless (b) Tolerance to noise (c) Harmonic distortion (d) Interharmonic distortion (e) Decaying harmonic and DC decaying offset (f) Amplitude step (g) Phase step (h) Amplitude and phase modulation (i) Frequency ramp response.

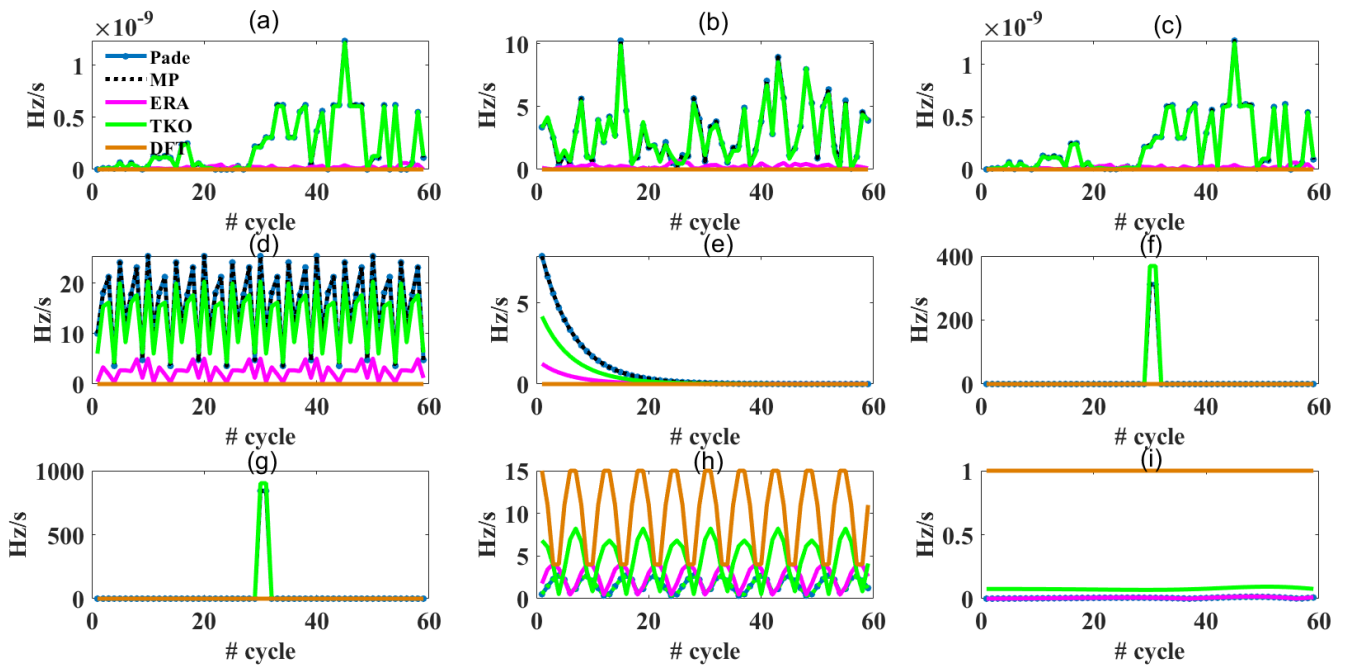


Fig. 3. RFE for the signals under study: (a) Noiseless (b) Tolerance to noise (c) Harmonic distortion (d) Interharmonic distortion (e) Decaying harmonic and DC decaying offset (f) Amplitude step (g) Phase step (h) Amplitude and phase modulation (i) Frequency ramp response.

IV. IMPLEMENTATION AND RESULTS UNDER REAL CONDITIONS

To test the algorithms under realistic conditions, a measurement system with current and voltage sensors [15, 16] and a Particle® WiFi IoT board [17] was designed. This system, referred to as IoTBPMU (Internet of Things Based Phasor Measurement Unit), is shown in Fig. 4, summarizing its main components, wiring diagram, and final assembly. The design is available at [18].

A. WEB INTERFASE DESIGN

Particle® boards possess their own Back-End (BE) allowing Over The Air (OTA) programming. This BE presents the variable computed by the board using the MQTT messaging protocol. Therefore, this variable can be easily recovered via the JavaScript (JS) environment or recovered by an IoT server such as: Thingspeak®, Ubidots®, or Nodered®; to mention a few. Thus, with this idea, an interface for displaying the measurements was designed, whose general structure is shown in the block diagram of Fig 5.

Function of the BE such as *Particle.variable* is efficient and robust for this kind of phasor monitoring application since its latency is one second. This function takes two parameters: the name of the variable that can be retrieved by the Particle cloud, and the name of the local variable stored/computed in the board. For each parameter a variable is required.

It should be emphasized that the html programming language permits to develop customized interfaces to visualize the variables in a friendly way being the best option for the development here presented. Full code for the Photon board based on the four-samples Padé method is available at [19]. Using the open libraries mentioned in [20], a web interface to visualize the measurements was developed, that is accessed to the public address at [21].

B. RESULTS

As a final test, the system was connected to a single phase of 127 VAC 60 Hz low voltage distribution network. Fig. 6 depicts the IoTBPMU in this situation. Fig. 7 shows the results given for the phasor parameters along with the Padé coefficients.

From Fig. 7a, the phasor parameters derived from the signal closely align with the expected values for this voltage level, confirming the accuracy of the proposed method in real-world low-voltage applications. The frequency is determined with minimal error, which demonstrates the algorithm's reliability in maintaining accurate measurements even in dynamic environments. The voltage peak is observed around 180 V, which is consistent with typical low-voltage distribution network levels. The phase shows slight variations, as expected, since the phasor parameters are updated every second, reflecting the real-time nature of the system's measurements. From the Padé coefficient behavior, it is observed that (See Fig. 7b) the q_1 coefficient exhibits a minimal variation because the frequency of the voltage is constant. In a similar way, the value of the q_2 coefficient is approximately equal to unity, thus indicating that the voltage signal does not have damping. This suggests that the signal's dynamic characteristics are well-preserved and accurately reflected in the computed parameters.

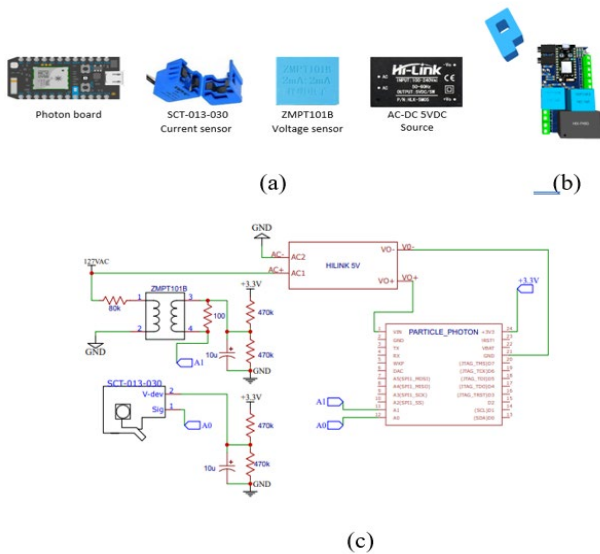


Fig. 4. The measurement system: (a) Main components, (b) System mounted, (c) Wiring diagram.

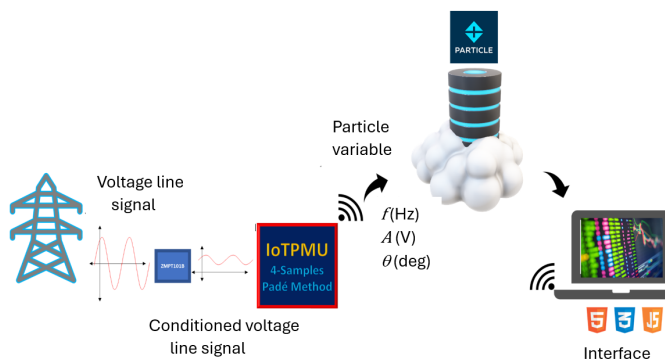


Fig. 5. Overall structure for measurement, publishing and remote displaying phasor information of the signal.



Fig. 6. IoTBPMU device installed at 127 VAC level.

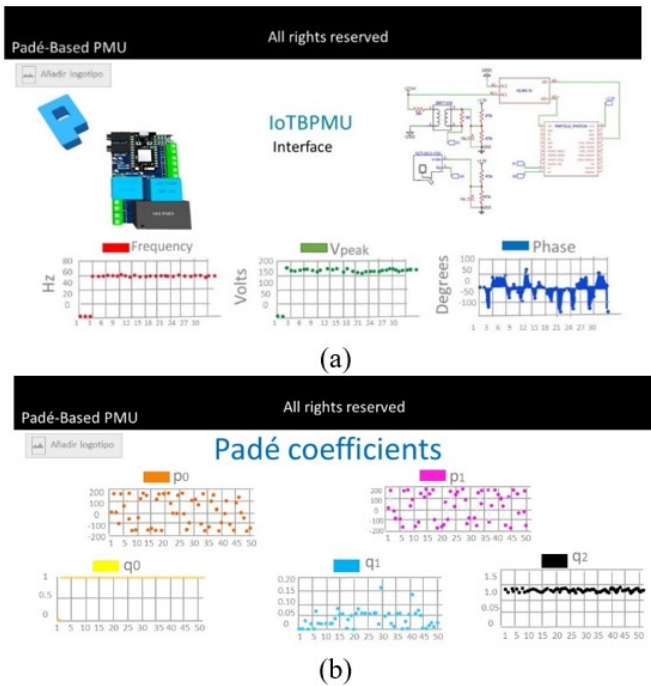


Fig. 7. The monitoring interface: (a) Phasor parameters, (b) Padé coefficients.

V. CONCLUSIONS

Implementing phasor estimation algorithms on IoT boards is typically challenging due to the complexity of the algorithms and the limited memory and processing capacity of such devices. However, this work demonstrates that the proposed Padé approximation-based algorithm can be easily implemented on IoT boards with minimal hardware resources, making it a cost-effective solution.

The results obtained from synthetic signals show that the algorithm complies with the IEEE C37.118 standard, confirming its accuracy and robustness in comparison to other methods such as ERA and MP. Although some deviations were observed in the presence of distorted signals, particularly with harmonics and interharmonics, the results are promising across most test cases. This highlights the need for further research to enhance the algorithm's performance under signal distortion, aiming to minimize TVE, FE, and RFE.

Additionally, the IoTBPMU system design is not only cost-effective but also highly replicable, thanks to its minimal hardware requirements and the availability of open-source code. This makes it accessible for a wide range of applications, from academic research to industrial monitoring systems. The use of IoT-based platforms provides scalability, allowing for easy integration into smart grid systems and enabling real-time phasor measurement with minimal latency.

The full implementation, including the web interface for real-time monitoring, demonstrates the system's practicality in

real-world scenarios, as evidenced by successful tests on low-voltage distribution networks. Moving forward, increasing the sample rate to better handle harmonic distortions and ensuring the algorithm's reliability under various grid conditions would be key steps toward enhancing its effectiveness. The simplicity of the system, combined with its ability to deliver accurate measurements, positions it as a viable solution for low-cost, real-time phasor monitoring in modern energy systems.

ACKNOWLEDGEMENTS

Authors with CVU numbers 88193, 30951, 211801, and 230004 gratefully acknowledge the support of the Mexican National Council for Humanities, Science, and Technology (CONACYT) through the National System of Researchers program (SNI). The authors also extend their thanks to Particle Inc. for the donation of boards through the Particle for Education program.

REFERENCES

- [1] Sarasij Das, Tarlochan Sidhu, "A Simple Synchrophasor Estimation Algorithm Considering IEEE Standard C37.118.1-2011 and Protection Requirements", *IEEE Tran. on Instr. and Meas.*, Vol. 62, No. 10, 2013, pp. 2704-2715.
- [2] Guglielmo Frigo, Paolo Attilio Pegoraro and Sergio Toscani, "Low-Latency, Three-Phase PMU Algorithms: Review and Performance Comparison", *MDPI Applied Sciences*, 2021, 11, 1-34.
- [3] Frigo, G.; Derviškić, A.; Zuo, Y.; Paolone, M. PMU-Based ROCOF Measurements: Uncertainty Limits and Metrological Significance in Power System Applications. *IEEE Trans. Instrum. Meas.* 2019, 68, 3810–3822.
- [4] Bartłomiej Arendarski, Steffen Rabe, Wolfram Heineken, Przemysław Komaricki, "Measurement accuracy verification of phasor measurement unit with dynamic phasor estimation", *Archives of Electrical Engineering*, 2018, 67, 529-543.
- [5] Yashasvi Bansal, Ranjana Sodhi, "A Half-Cycle Fast Discrete Orthonormal S Transform based Protection-class μ PMU", DOI 10.1109/TIM.2020.2980339, *IEEE Transactions on Instrumentation and Measurement*.
- [6] David A. Kaiser, James F. Kaiser, "Estimation of Power Systems Amplitudes, Frequencies, and Phase Characteristics using Energy Operators", 2012.
- [7] Jalal Khodaparast and Mojtaba Khederzadeh, "Least square and Kalman based methods for dynamic phasor estimation: a review", *Protection and Control of Modern Power Systems*, 2017, 2-18.
- [8] R. Ghiga, Q. Wu, K. Martin, W. Z. El-Khatib, L. Cheng and A. H. Nielsen, "Dynamic PMU Compliance Test under C37.118.1aTM-2014", *IEEE*.
- [9] T. Bi, H. Liu, Q. Feng, C. Qian and Y. Liu, "Dynamic Phasor Model-Based Synchrophasor Estimation Algorithm for M-Class PMU," in *IEEE Transactions on Power Delivery*, vol. 30, no. 3, pp. 1162-1171, June 2015, doi: 10.1109/TPWRD.2014.2353816.
- [10] JA. Zamora-Mendez, F. Zelaya-A., J. A. de la O Serna, J. H. Chow, and M. R. Arrieta Patemina, "Model-based synchrophasor estimation by exploiting the eigensystem realization approach," *Electric Power Systems Research*, vol. 189, p. 106249, 2020, doi: 10.1016/j.epsr.2020.106249.
- [11] L. Wang and J. Suonan, "A Fast Algorithm to Estimate Phasor in Power Systems," *IEEE Trans. Power Del.*, vol. 30, no. 2, pp. 1-10, Mar. 2015, doi: 10.1109/TPWRD.2014.2342242.
- [12] IEEE Standard Association. IEEE Standard for Synchrophasor Measurements for Power Systems—Amendment 1: Modification of Selected Performance Requirements, in *IEEE Std C37.118.1a-2014; Amendment to IEEE Std C37.118.1-2011*; IEEE Power & Energy Society: Piscataway, NJ, USA, 2014; pp. 1–25

- [14] R.J. Betancourt, E. Barocio, C.M. Rergis, J.M. González-López, A.C. Sánchez. A spatio-temporal processing Padé approach for visualizing harmonic distortion propagation on electrical networks *Electr Power Syst Res*, 203 (2022), p. 107643
- [15] YHDC. Available: <http://en.yhdc.com/product1311.html?productId=703> (accessed on 5 June 2023).
- [16] InnovatorsGuru. (2019). ZMPT101B: Micro Precision Voltage Transformers [Data sheet]. <https://innovatorsguru.com/wp-content/uploads/2019/02/ZMPT101B.pdf> (accessed on 5 December 2024).
- [17] Particle Inc. Available online: <https://store.particle.io/collections/wifi> (accessed on 5 June 2023).
- [18] PCB Padé-based PMU. Ramon Betancourt. Available online: https://oshwlab.com/rjimenez_3992/iotpmu.
- [19] C code of four-samples Padé method. Ramon Betancourt. Available online: https://go.particle.io/shared_apps/63e68811b8500f06aa6b03e5.
- [20] The Free and Open-Source CDN. Available online: <https://cdnjs.com/>
- [21] Web interface of Padé-based PMU. Ramon Betancourt. Available online: <https://sites.google.com/ucol.mx/pad-based-pmu/phasor-characteristics>

National Research System. His research interests include modeling, simulation, control, and stability in power systems, power quality, virtual instrumentation, and the application of IoT technology in power systems.



EMILIO BAROCIO Received the M.E. degree from the University of Guadalajara, Guadalajara, México, in 1998, and the Ph.D. degree from CINVESTAV, Guadalajara, in 2003, both in electrical engineering. He is currently a Researcher/Professor with the Department of Mechanical and Electrical Engineering, University of Guadalajara. Dr. Barocio was a recipient of the Arturo Rosenblueth Award for the best Ph.D. thesis on Science and Technology of México in 2003.. He was distinguished with the Marie-Curie Incoming International Fellowship at the Imperial College of London in 2013. He was also a recipient of with the IEEE Power Energy Society and Power System Dynamic Performance Committee Prize Paper Awards in 2018. He has been also a visiting professor in the EPS and SG Lab at the Zurich University of Applied Sciences ZHAW, Winterthur, Switzerland in the summer of 2018 and 2019, respectively.



JUAN M. GONZALEZ He received the B.S. degree in Electrical Engineering from the University of Colima, Colima, Mexico, in 2004, and the M.Sc. and Ph.D. degrees in Electrical Engineering from CINVESTAV, Guadalajara, Mexico, in 2006 and 2010, respectively. From 2010 to 2017, he held various teaching positions at the Technological University of Manzanillo, Mexico. From 2008 to 2009, he was a Visiting Student at the University of Waterloo, Waterloo, ON, Canada, and a Postdoctoral Fellow from 2011 to 2012, working on smart grid topics. He joined University of Colima in 2017 as a Full-Time Professor. His research interests include modeling, simulation, control, stability in PES, smart homes, renewable energy, and engineering teaching methodologies using AMR VMR.



ANTONIO CONCHA SANCHEZ Received the Ph. D. degree in automatic control from the Center of Research and Advanced Studies of the National Polytechnic Institute, in 2013, from 2014 to 2015, he was a Postdoctoral Researcher with the National Autonomous University of Mexico, Mexico City. Since 2016, he has been a Professor with the Faculty of Mechanical and Electrical Engineering, University of Colima, Colima, Mexico. His current research focuses on system identification, control theory, and vibration control. He is a member of the Mexican National Research System.

BIOGRAPHIES



MARCO A. PEREZ G. Received his M.S. degree in 2001 from the Centre for Research and Advanced Studies (CINVESTAV) at the National Polytechnic Institute (IPN), Mexico. Since 2000, he has been serving as an Associate Professor in the Faculty of Electromechanical Engineering at the University of Colima. His research interests encompass the development of digital educational resources; modeling, simulation, control, stability and the application of IoT technologies in power systems. He is currently pursuing a doctoral degree in Information Technologies.



RAMON JIMENEZ BETANCOURT Received the M.S. degree in 1999 and the Ph.D. degree in 2007 from the Centre for Research and Advanced Studies (CINVESTAV) of the National Polytechnic Institute (IPN) of Mexico. Since 1999 he is an Associate Professor in the Faculty of Electromechanical Engineering, University of Colima, Manz. Dr. Betancourt is a member of the Mexican